

Chapter 4

Graphene for Transparent Electrodes and Organic Electronic Devices

Xiangjian Wan, Guankui Long and Yongsheng Chen

Abstract Graphene has been regarded as a promising material in organic electronics owing to its outstanding electronic, optical, thermal, and mechanical properties. In this chapter, first, we summarize and discuss the application of graphene as transparent electrode in organic photovoltaic (OPV) cells and organic light emitting diodes (OLED). Improving the conductivity of graphene without compromising the transparency and tuning its work function to match the interface and/or active materials are proposed to focus on the future study for graphene-based transparent electrode. Then, the application of graphene as acceptor material in OPV has been addressed. The factors of size, energy level, and functionalization of graphene should be considered first. Last, graphene-based all-carbon electronics have been introduced, which indicates that graphene exhibits great potential for fabricating the highly demanded all-carbon, flexible devices and electronics.

4.1 Introduction

Graphene, a single sheet composed of sp^2 -hybridized carbon, is regarded as the basic building block of all dimensional graphitic materials; it can be stacked to form 3D graphite, rolled to form 1D nanotubes, and wrapped to form 0D fullerenes. In recent years, graphene has been of great interests owing to its outstanding electronic, optical, thermal, and mechanical properties [1, 2]. Due to its unique and superior optical and electronic properties such as good transparency, high

X. Wan · G. Long · Y. Chen (✉)

Key Laboratory of Functional Polymer Materials and the Centre of Nanoscale Science and Technology, Institute of Polymer Chemistry, College of Chemistry, Nankai University, Tianjin 300071, China
e-mail: yschen99@nankai.edu.cn

mobility, high electrical conductivities, and low contact resistance with organic materials, graphene has been extensively studied in the field of organic electronic devices [2], such as organic photovoltaics (OPVs) [3–5], organic light-emitting diodes (OLEDs) [6, 7], field effect transistors (FETs) [8, 9], and etc. There are quite some broad reviews about graphene in many aspects [10–15]. Herein, we will restrict ourselves to summarize and discuss transparent electrodes based on graphene and application of graphene in the electronic devices, especially our works for OPVs.

4.2 Graphene for Transparent Electrode

As the essential part of optoelectronic devices, the ideal transparent electrodes should have high transparency, low sheet resistance, proper work function, and low preparation cost. Currently, indium tin oxide (ITO) plays a dominant role and is the market standard for most of transparent electrode applications. However, the use of ITO as transparent electrode may be limited for its intrinsic drawbacks such as the costly preparative methods (sputtering, evaporation, pulsed laser deposition, and electroplating), limited source of indium on the Earth, toxic property of indium for environment and humans, its intrinsic brittleness property, etc. Thus, developing new transparent conducting materials has become necessary. Graphene-based transparent electrodes have drawn great attentions owing to its excellent properties such as high mobility, high transparency, etc. Several excellent reviews have discussed the updated progress and comprehensive applications of the transparent electrodes based on graphene [16, 17]. Herein, we will give a brief summarization of the graphene-based transparent electrode for organic electronic devices, especially for OPVs.

4.2.1 *Transparent Electrode Based on rGO*

In contrast with graphene based on other preparation methods such as micromechanical exfoliation [18], epitaxial growth [19], and chemical vapor deposition (CVD) [20], reduced graphene oxide (rGO) [21–23] has been studied primarily owing to the advantages of high throughput preparation, low cost, and the simplicity of the fabrication technique.

In our initial work, we have studied spin-coated GO thin films by different reduction treatments with hydrazine reduction and/or high-temperature annealing, producing films with sheet resistances as low as 10^2 – 10^3 Ω /sq with 80 % transmittance for 550 nm light (Fig. 4.1a) [24]. Using the neat rGO film as the transparent anode, we have demonstrated solution-processed polymer OPVs with poly-(3-hexylthiophene) (P3HT) as the electron donor and phenyl-C₆₁-butyric acid methyl ester (PCBM) as the acceptor (Fig. 4.1b) [25]. After spin-coating

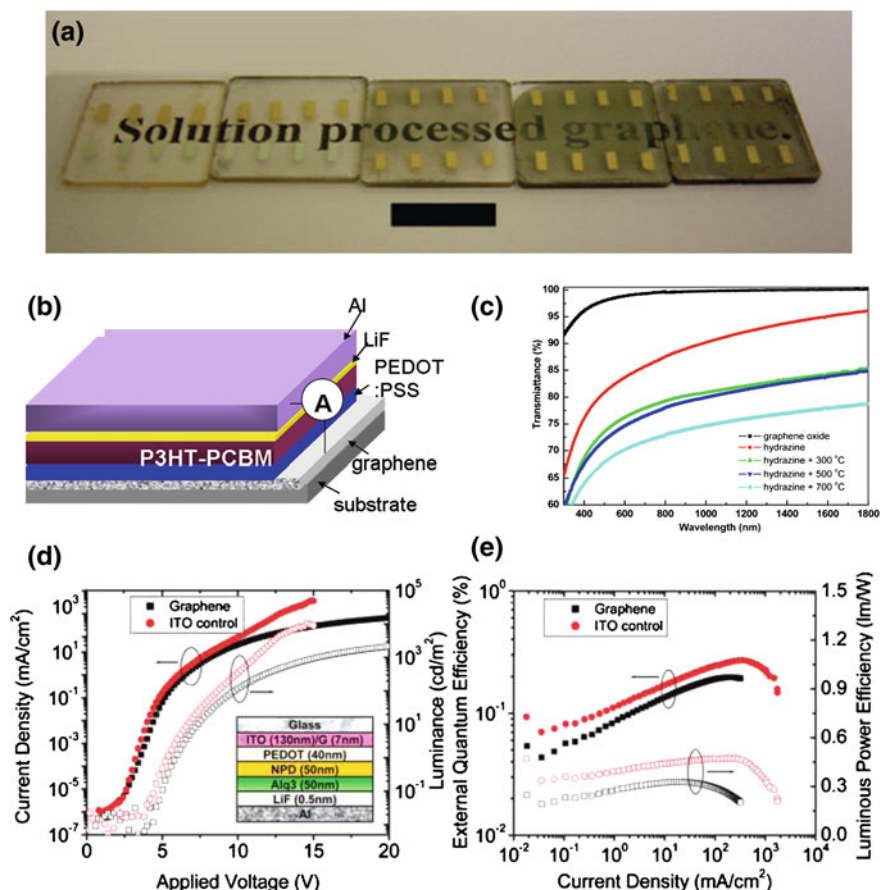


Fig. 4.1 (a) Photograph of an unreduced (*left most*) and a series of high-temperature reduced GO films of increasing thickness. Black scale bar is 1 cm. (b) Device structure and energy diagram of the fabricated device with structure quartz/graphene/PEDOT:PSS/P3HT:PCBM/LiF/Al. (c) Optical transmittance spectra of graphene oxide film (~ 40 nm) and graphene films (~ 25 nm) with different reduced methods. (d) Current density (*filled symbols*) and luminance (*open symbols*) versus applied forward bias for an OLED on graphene (*squares*) and ITO (*circles*), with OLED device structure anode/PEDOT:PSS/NPD(50 nm)/Alq₃(50 nm)/LiF/Al as shown in the inset. (e) External quantum efficiency (EQE) (*filled symbols*) and luminous power efficiency (LPE) (*open symbols*) for an OLED on graphene film (*squares*) and ITO glass (*circles*). (a) Reproduced with permission [24]. Copyright 2008, ACS. (b–c) Reproduced with permission [25]. Copyright 2010, Elsevier. (d–e) Reproduced with permission [6]. Copyright 2010, ACS

deposition, the insulating graphene oxide films were reduced through exposure to hydrazine vapor and then annealed under inert conditions to render the material electrically conductive. The electrical conductivity of the as-prepared graphene film is closely related to the annealing temperature. At a given film thickness of ~ 25 nm, graphene film conductivity increased with the increase of the annealing

temperatures (Fig. 4.1c). The reduced graphene films could have a sheet resistance of 17.9 K Ω /sq (transmittances of 69 % at 550 nm) and a conductivity of 22.3 S/cm. The OPV device under illumination of simulated solar light (AM 1.5G) shows a short-circuit photocurrent density (J_{sc}) of 1.18 mA/cm² with an open-circuit voltage (V_{oc}) of 0.46 V, a filling factor (FF) of 0.25, and PCE of 0.13 %. The low PCE is due to the high sheet resistance of graphene films and the hydrophobic graphene film surface, which makes it rather hard to get a uniform PEDOT:PSS layer.

Wu et al. used rGO as transparent conductive anodes for an organic bilayer small molecule OPV cells [26]. The transparent electrodes based on graphene were obtained by vacuum annealing of graphene oxide or by a combination of a hydrazine treatment and argon annealing at 400 °C. The thickness of graphene films used to fabricate OPV cells is between 4 and 7 nm, and the corresponding values of the transmittance and sheet resistance are 95–85 %, and 100–500 k Ω /sq, respectively. Devices with structure of anode/CuPc/C₆₀/BCP/Ag were fabricated. The J_{sc} , V_{oc} , FF, and PCE are 2.1 mA/cm², 0.48 V, 0.34, and 0.4 %, respectively, for the cell on graphene, and 2.8 mA/cm², 0.47 V, 0.54, and 0.84 %, respectively, for the cell on ITO for comparison. The poor solar cells performance is mainly caused by the high sheet resistance of the graphene thin films, which need to be reduced without compromising transmittance.

Wu et al. also demonstrate OLEDs with solution-processed graphene film as transparent conductive anodes (Fig. 4.1d, e) [6]. The graphene electrodes were deposited on quartz substrates by spin coating of an aqueous dispersion of functionalized graphene, followed by a vacuum anneal step to afford the graphene films with resistance and transmittance of 800 Ω /sq and 82 % (550 nm). OLED device with structure of anode/PEDOT:PSS/N,N'-di-1-naphthyl-N,N'-diphenyl-1,1'-biphenyl-4,4'-diamine(NPD)/tris(8-hydroxyquinoline)aluminum(Alq₃)/LiF/Al was fabricated. The OLEDs on graphene exhibited a current drive and light emission intensity comparable to those of ITO-based devices when the current density was <10 mA/cm². Meanwhile, the external quantum efficiency (EQE) and the luminous power efficiency (LPE) of graphene-based OLEDs nearly matched that of the ITO-based device. The turn-on voltage of the OLED with graphene-based transparent electrode was 4.5 V, slightly higher than the 3.8 V of the ITO-based device.

Similar, works have been reported and comparable PCE results were achieved using rGO as transparent electrode in OPVs. For example, Eda et al. reported the preparation of transparent and conductive graphene film by vacuum filtration of graphene oxide to form a film, followed by a combination of hydrazine vapor and low-temperature annealing (200 °C) in nitrogen or vacuum [27]. Using above rGO film as the transparent electrode, OPV device with P3HT and PCBM as active layer gave the PCE of approximately 0.1 %, which is limited by the large resistance with the order of 10⁵ Ω /sq for the rGO electrodes. Yin et al. fabricated flexible OPV devices by using a transferred rGO film as the transparent electrode. The highest PCE obtained is 0.78 %, employing the flexible rGO/polyethylene terephthalate (PET)-based transparent electrodes with a transparency of 55 % and resistance of 1.6 k Ω /sq [28]. Geng et al. reported the preparation of transparent

conductive graphene films by a two-step reduction method that consisted of the controlled chemical reduction of GO in an aqueous suspension and the thermal annealing of the resultant films [29]. OPV devices with P3HT and PCBM as active layer showed PCE of 1.01 %.

4.2.2 Transparent Electrode Based on CVD graphene

CVD is an important and successful method to obtain high-quality graphene films [30–32]. Recently, films with sheet resistance of 280 Ω/sq (80 % transparency) and 770 Ω/sq (90 % transparency) have been reported for CVD graphene synthesized on Ni films [20].

Wang et al. synthesized a large-area graphene film on Ni-coated SiO_2/Si wafer using a CVD process [33]. For 6–30 nm thick graphene films, the average sheet resistance varies from 1350 to 210 Ω/sq with an optical transparency from 91 to 72 % in the visible light wavelength range. As shown in Fig. 4.2, a BHJ structure solar cell using the graphene anode was fabricated. The J_{sc} , V_{oc} , FF, and PCE are 2.39 mA/cm^2 , 0.32 V, 0.27, and 0.21 %, respectively. The poor performance was caused by the hydrophobic property of graphene, which could not form the uniform coating of PEDOT:PSS. After the UV treatment of graphene film for 10 min to improve the surface wettability, the device PCE was increased to 0.74 %. In order to avoid the disruption of the aromatic structures caused by covalent bonding with oxygen groups after the UV treatment, the graphene anode was modified by self-assembled pyrene buanoic acid succidymidyl ester (PBASE). A well-improved performance ($V_{oc} = 0.55$ V, $J_{sc} = 6.05$ mA/cm^2 , FF = 0.51, and PCE = 1.71 %) was obtained. In contrast, the device made with ITO anode showed V_{oc} , J_{sc} , FF, and PCE of 0.56 V, 9.03 mA/cm^2 , 0.61, and 3.10 %, respectively.

Similar works employing CVD graphene as transparent electrode for OPV application have been reported recently. For example, Arco et al. reported a transparent graphene film by CVD with sheet resistance 230 Ω/sq and 72 % transparency at the wavelength of 550 nm [34]. OPV devices using CVD graphene and ITO electrodes were fabricated side-by-side on flexible PET substrates and were confirmed to offer comparable performance, with PCE 1.18 and 1.27 %, respectively. Loh et al. reported a layer-by-layer (LBL) transfer method of CVD graphene sheets. The LBL, acid-doped, four layer graphene film exhibited a sheet resistance of 80 Ω/sq and a transmittance of 90 % at 550 nm, which is comparable to the ITO [35]. OPVs with the structure of graphene/PEDOT:PSS/P3HT:PCBM/LiF/Al exhibited the best performance with a PCE of 2.5 %, which is comparable with the PCE of 3 % for ITO-based devices. Lee and his coworkers reported the preparation of multilayer graphene (MLG) film grown by CVD [36]. OPV devices using graphene with sheet resistances of 606 Ω/sq and transmittances of 87 % as electrodes showed the best performance with PCE up to 2.58 ± 0.45 %.

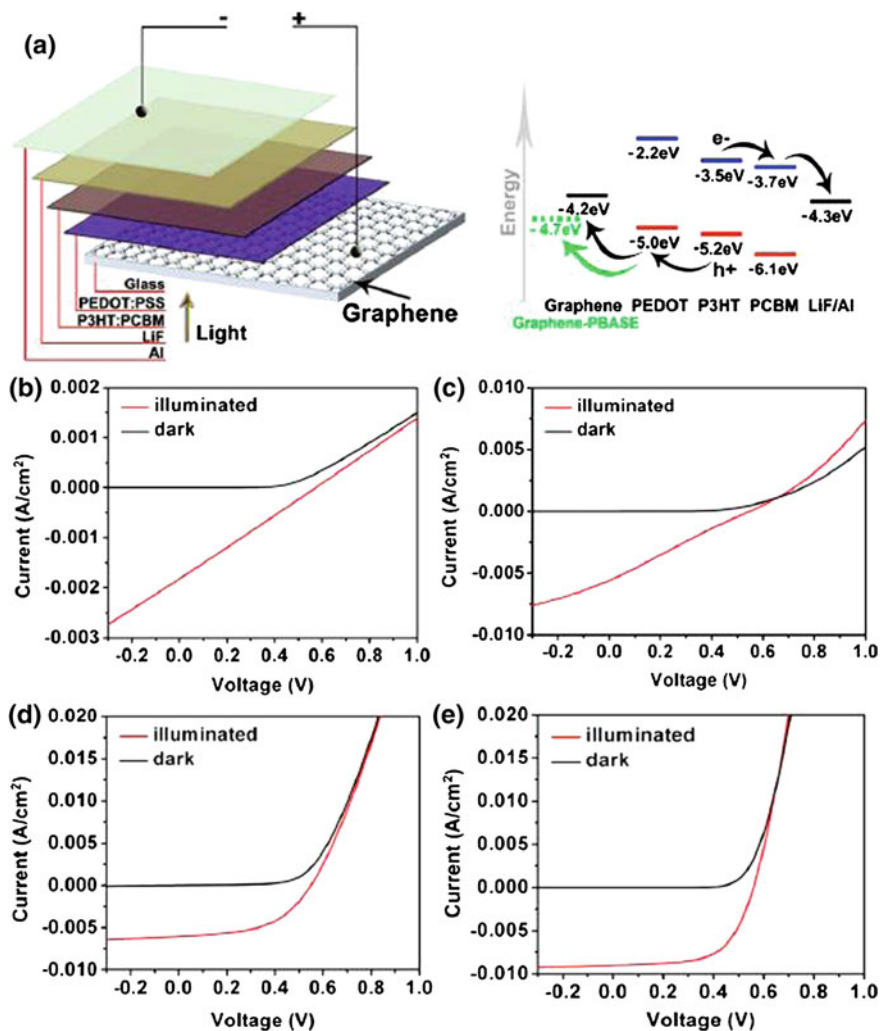


Fig. 4.2 (a) Energy diagram of the fabricated device with structure graphene/PEDOT:PSS/P3HT:PCBM/LiF/Al. (b–e) Current voltage characteristics of the photovoltaic devices based on graphene films in *dark* and under illumination, where (b) is from pristine graphene film, (c) graphene film treated by UV light, (d) graphene film modified by PBASE, (e) ITO anode for comparison. Reproduced with permission [33]. Copyright 2009, AIP

4.2.3 Improving the Conductivity of Graphene-Based Transparent Electrode

The high sheet resistance is one of the most important factors for the poor performance of organic electronic devices employing transparent electrodes based on graphene. A strategy to improve the conductivity of the graphene films is to

incorporate a conductive material into them. Chen et al. have reported a hybrid material prepared from graphene and poly(3,4-ethyldioxythiophene) (PEDOT) [37], which showed good transparency and electrical conductivity flexibility together with high thermal stability and was easily processed in both water and organic solvents (Fig. 4.3a, b). Conductivities of 0.2 S/cm and light transmittance of greater than 80 % in the 400–1800 nm wavelength range were observed for films with thickness of tens of nm. In the view of the vacancies and topological defects on the rGO sheet owing to the release of oxygen-containing functional groups, another strategy to improve the conductivity is to repair the defects. Liu et al. reported a method for real-time repair of the newborn vacancies by introducing carbon radicals in the thermal annealing process via a rapid-heating process (Fig. 4.3c–f) [38]. The sheet conductivity of thus-obtained single-layer graphene was raised more than sixfold to 350–410 S/cm (while retaining >96 % transparency). This method provides a simple and efficient process for obtaining highly conductive transparent graphene films. Considering the high conductivity of carbon nanotubes, Tung et al. reported a hybrid nanocomposite comprised rGO and carbon nanotubes (G-CNT) (Fig. 4.3g) [39]. By introducing CNTs, the conductivity of the hybrid material was enhanced, while sacrificing little in transparency. G-CNT film by spin coating with sheet resistance of 240 Ω /sq and 86 % transmittance was obtained. In addition, G-CNT hybrid film exhibited better mechanical stabilities than ITO. In a comparison experiment, after bending to 60° more than 10 times, the resistance of the brittle ITO film increased by three orders of magnitude, while the G-CNT electrode remained nearly unchanged. P3HT:PCBM BHJ device using G-CNT hybrid material as the transparent electrode exhibited a PCE of 0.85 %. The J_{sc} , V_{oc} , and FF were 3.47 mA/cm², 0.583 V, and 0.42, respectively. The low J_{sc} and FF are likely due to poor contact at the interface between the G-CNT and the polymer blend.

4.2.4 Tuning the Work Function of Graphene-Based Transparent Electrode

In organic electronic devices, work functions of electrodes play an important role and have to be tuned to minimize the energy barriers for charge injection/extraction and improve the device performance. For example, in the common OPV device, the work function of ITO anode should be improved to match with the HOMO of the donor. UV–ozone treatment can improved the work function of ITO, however, a PEDOT:PSS layer with high work function (5.2 eV) are still need to facilitate the hole transfer as well as improve the surface quality. For graphene, its work function is presumed to be 4.5 eV [40]. However, the work function of graphene is variable according to the different sizes, layer structures, functionalizations, doping, and surface modification. Recently, Hang et al. reported to use alkali carbonates to dope the rGO-SWCNT composites and modify their work functions [41]. The doping and work functions were characterized by XPS (Fig. 4.4a). A clear trend

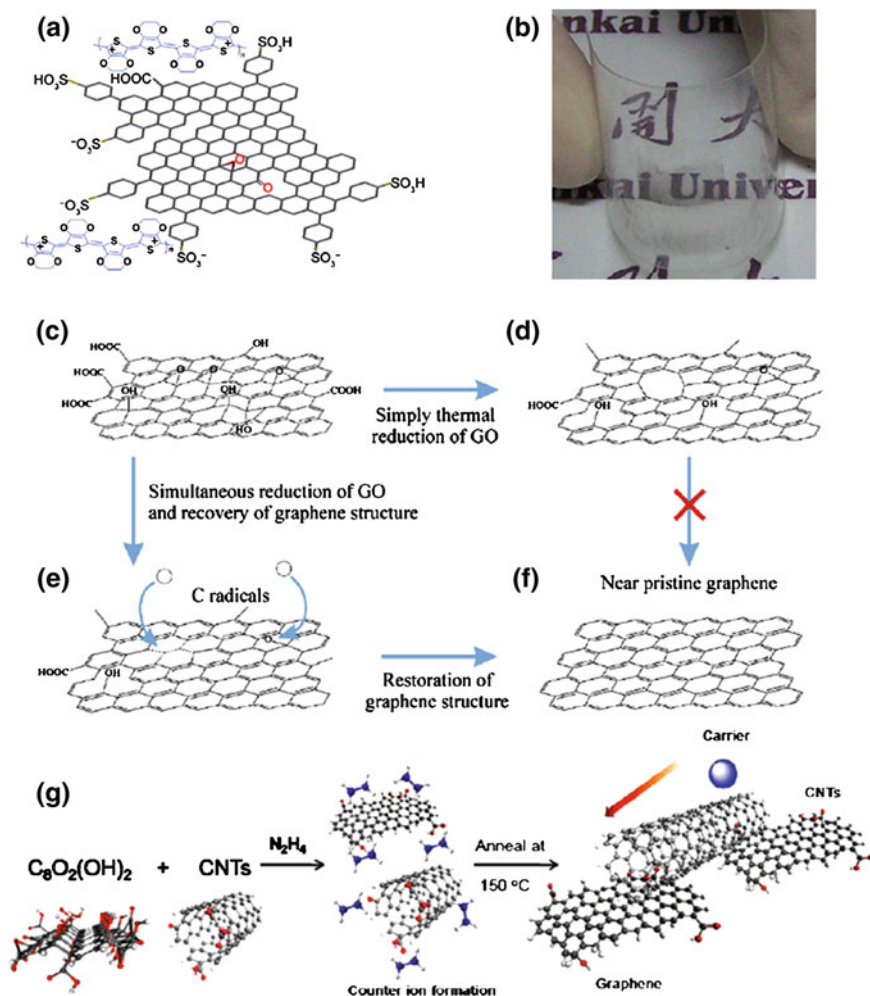


Fig. 4.3 (a) Schematic representation of part of the structure of graphene-PEDOT. (b) A picture of a graphene-PEDOT film with a thickness of ~ 32 nm on a transparent PMMA substrate. (c–f). Structure of GO (c) and thermally reduced GO (d); Simultaneous reduction of GO and recovery of graphene structure (e), to obtain near pristine graphene (f). (g) Scheme of the composite of CNT and GO. (a–b) Reproduced with permission [37]. Copyright 2009, Springer (c–f) Reproduced with permission [38]. Copyright 2011, (g) Reproduced with permission [39]. Copyright 2009, ACS

was observed: the values of Φ_w of the rGO-SWCNT electrodes decreased from 4.6 eV when doped with Li_2CO_3 to 3.4 eV when doped with Cs_2CO_3 (Fig. 4.4b). The formation of interfacial dipoles was presumed to be the reason for decreasing the work function of the rGO-SWCNT composites. Inverted P3HT/PCBM solar cells employing Cs_2CO_3 doped rGO-SWCNTs as transparent electrode (transparency 65.8 % at 550 nm and sheet resistance 331 Ω/sq) was fabricated and gave

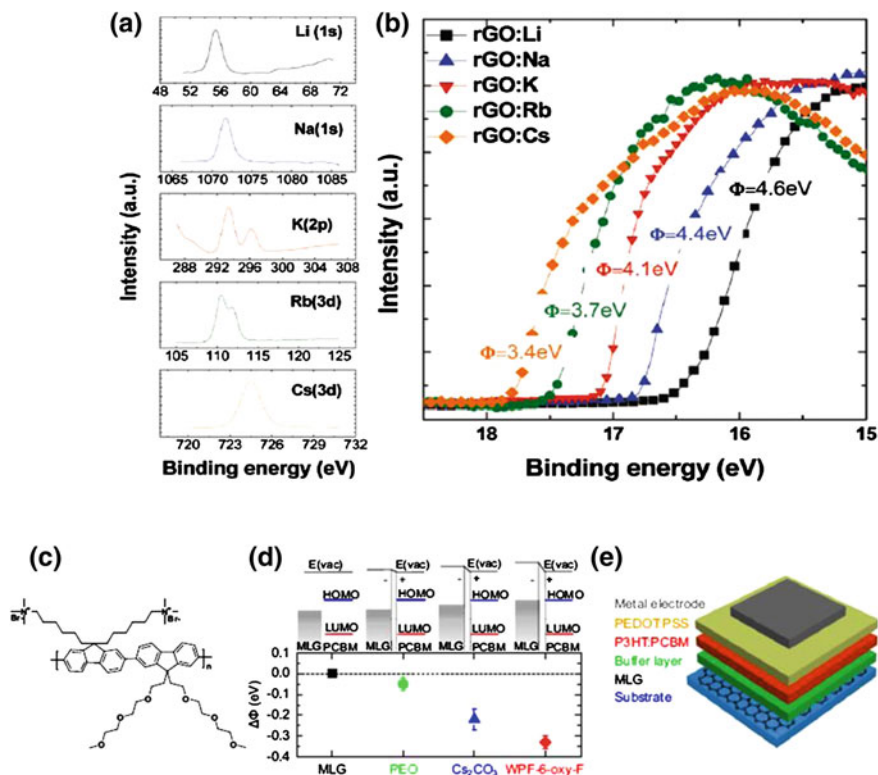


Fig. 4.4 Measurements of the values of Φ_w of the rGO-SWCNT films after doping with various alkali carbonates. (a) XPS and (b) UPS spectra of the rGO doped with various alkali carbonates. The pronounced peaks for the alkali metals indicate the successful doping of the alkali carbonates. The work functions of the rGO-SWCNT films after doping with Li_2CO_3 and Cs_2CO_3 were 4.6 and 3.4 eV, respectively. The values of Φ_w of the rGO-SWCNT films were determined from the UPS secondary electron cutoff. (c) Molecular structure of WPF-6-oxy-F. (d) Changes to the effective work functions of MLG films with interfacial dipole layers. (e) Schematics of an inverted-structure OPV with the work-function-engineered MLG electrode. (a–b) Reproduced with permission [41]. Copyright 2011, ACS (c–e) Reproduced with permission [42]. Copyright 2010, AIP

PCE of 1.27 %, which is comparable with that of the normal structure device. Lee and his coworkers reported that the work function of MLG film grown by CVD could be tuned by using thin interfacial dipole layers [42]. First, the MLG film was transferred to the glass substrate, and one of the following three types of interfacial dipole layers was spin coated onto it: 0.1 wt% solution of poly(ethylene oxide) (PEO) in methanol, 0.2 wt% solution of Cs_2CO_3 in 2-ethoxyethanol, or 0.2 wt% solution of poly[9,9-bis((6'-(N,N,N-trimethylammonium)hexyl)-2,7-fluorene)-alt-(9,9-bis(2-(2-(2-methoxyethoxy) ethoxy)ethyl)-9-fluorene))]dibromide (denoted as WPF-6-oxy-F, Fig. 4.4c) in methanol. The work function of the untreated MLG film was 4.58 ± 0.08 eV, it could be modified when different interfacial dipole

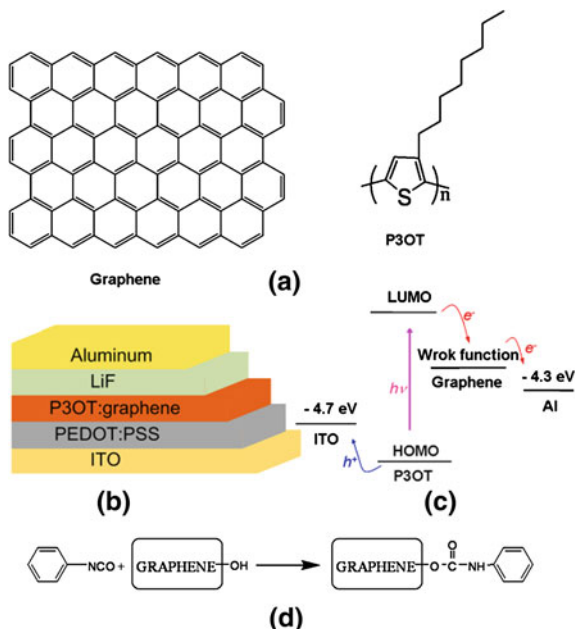
layers were used: 0.05 ± 0.03 eV with PEO, 0.22 ± 0.05 eV with Cs_2CO_3 , and 0.33 ± 0.03 eV with WPF-6-oxy-F (Fig. 4.4d). As transparent cathode in inverted OPV device, WPF-6-oxy-F doping MLG film was found to be the best material because its work function had been reduced to be close to the LUMO of PCBM. It is to note that WPF-6-oxy-F had a negligible effect on the absorption properties of the MLG film in the visible wavelengths because the energy gap of WPF-6-oxy-F lies in the UV wavelength range. BHJ device with an inverted structure (Fig. 4.4e) MLG/WPF-6-oxy-F/P3HT:PCBM/PEDOT:PSS/Al gave PCE 1.23 %, which was almost half of the PCE 2.23 % of cells with WPF-6-oxy-F functionalized ITO electrodes.

Although the initial results demonstrate that graphene films prove to be effective and exhibit great potential as transparent electrodes, significant improvement is needed for organic electronic devices employing graphene as the transparent electrodes. In future studies, improvement of the conductivity without sacrifice of the transparency should be first considered. In general, defects in the graphene sheets for both from rGO and from CVD are the main factors for low conductivity. Thus, reducing defects in the preparation process as well as combining with post-treatment are necessary. On the other hand, for device fabrication, the hydrophilicity of graphene films has to be improved or modified to allow for spin coating with hole-transporting layers such as PEDOT:PSS. Finally, for commercialization consideration, low-cost and large-scale production is preferred for the graphene-based transparent electrodes. In addition, roll-to-roll process is preferable for low-cost and large-scale production for OPVs. How to fulfill the requirement of roll-to-roll process is also a challenge for graphene-based transparent electrodes.

4.3 Graphene for Acceptor Material in OPVs

Currently, the most successful organic solar devices are fabricated in BHJ structure, with low band-gap polymers as the donor and fullerene derivatives such as PCBM as the acceptor. In contrast to the widely focused attentions on the design and synthesis of low band-gap donor materials [43, 44], unfortunately, few acceptor materials other than the fullerene derivatives have been developed. As the most widely used acceptor, C_{60} based acceptors have some limits [45–47], e.g., very weak absorption in the visible range, low LUMO energy level which is hard to tune for high V_{oc} in BHJ devices. Although much efforts have been made on modifying fullerene and its derivatives, only limited improvement has been achieved. This has prompted studies for new acceptor materials with energy levels different from those of C_{60} derivatives, and wide versatility in terms of derivatization and functionalization [48, 49]. In view of its excellent electronic properties such as high mobility, tunable energy level, well dispersion ability in organic solution, etc., it is expected that graphene and its derivatives should be a good alternative acceptor material in OPVs.

Fig. 4.5 (a) The idealized chemical structures of graphene and P3OT. (b) Schematic of the device with P3OT/graphene thin film as the active layer and the structure ITO/PEDOT:PSS (40 nm)/P3OT:graphene (100 nm)/LiF (1 nm)/Al (70 nm). (c) Energy level diagram of P3OT and SPFGraphene. (d) Schematic representation of the reaction of phenyl isocyanate with graphene oxide to form SPF Graphene. (a–d) Reproduced with permission [4]. Copyright 2008, Wiley-VCH



Chen et al. have reported the fabrication and comprehensive studies of the BHJ structure solar cells employing solution processable functionalized graphene (SPF Graphene) as the acceptor and P3OT as the donor (Fig. 4.5) [4]. As shown in Fig. 4.6, the strong photoluminescence (PL) of P3OT is remarkably reduced after the introduction of SPF Graphene, showing that efficient energy transfer occurs along the P3OT–SPF Graphene interface. The PL quenching behavior has been in detail studied by Hill et al. through electrochemical studies of GO sheets and P3HT utilizing a surfactant-assisted method [50]. The efficient quenching of PL emission with GO indicates that graphene is a promising electron-accepting material for OPV applications. SPF Graphene-based solar cells by spin coating a dichlorobenzene solution with different ratios of SPF Graphene and P3OT have been studied in details. As shown in Table 4.1, the performance of the P3OT/SPFG-based photovoltaic device was much higher than that of the device based on pristine P3OT, indicating that there was an obvious charge transfer from P3HT donor to SPFGGraphene acceptor. Under simulated 100 mW AM 1.5G illumination, a PCE of 0.32 % for the P3OT/SPF Graphene-based devices with 5 % SPFGGraphene in the active layer was obtained. After annealing treatment, the performance of the devices is greatly improved. The device without annealing treatment had a PCE of only 0.32 %, V_{oc} of 0.56 V, J_{sc} of 2.5 mA/cm², and FF of 0.23. After annealing at 160 °C for 20 min, the PCE increased to 1.4 %, with V_{oc} , J_{sc} , and FF increasing to 0.92 V, 4.2 mA/cm², and 0.37, respectively. Two factors should contribute to the improvement of the device performance. During the annealing process, graphene sheet should be recovered at least partially again with

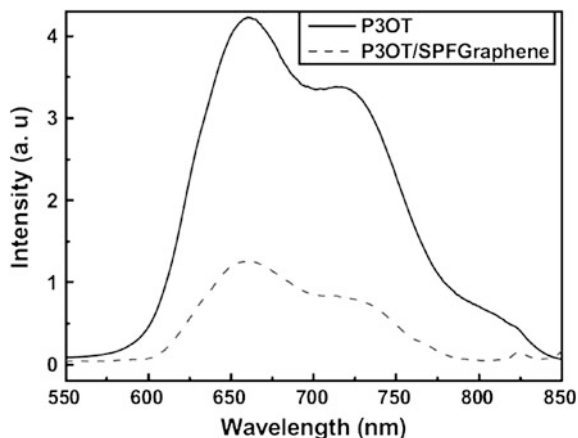


Fig. 4.6 PL spectra of P3OT and P3OT/SPF Graphene composite films at an excitation wavelength of 433 nm. The films were made by spin coating from solutions of P3OT (15 mg mL⁻¹) and P3OT/SPF Graphene (P3OT: 15 mg mL⁻¹, SPF Graphene content 5 %) at 2,000 rpm for 9 s. The films are ca. 100 nm thick. Reproduced with permission [4]. Copyright 2008, Wiley-VCH

Table 4.1 PV characteristics (V_{oc} , J_{sc} , FF, and PCE) of the devices with the structure ITO/PEDOT:PSS (40 nm)/P3OT:SPFGraphene 100 nm)/LiF (1 nm)/Al (70 nm) under simulated 100 mW AM 1.5G illumination, having different graphene content with different annealing treatment. Reproduced with permission [4]. Copyright 2008, Wiley-VCH

SPFGraphene content [%]	Annealing		V_{oc} (V)	J_{sc} (mA/cm ²)	FF	PCE %
	Temperature(°C)	Time(min)				
0	No		0.38	0.014	0.18	0.0095
1	No		0.38	0.54	0.26	0.052
1	160	10	0.94	0.37	0.24	0.083
5	No		0.56	2.5	0.23	0.32
5	160	10	0.98	3.2	0.32	0.98
5	160	20	0.92	4.2	0.37	1.4
5	210	10	1.0	3.2	0.31	0.98
15	No		0.38	0.35	0.24	0.034
15	160	10	0.92	0.35	0.25	0.080

the removal of the functional groups, resulting in improved charge transport mobility of these graphene sheets. In addition, the morphology of the P3OT matrix can be improved, during the annealing process, with an increase in degree of crystallinity and then an enhancement of the charge transport mobility. We also fabricated similar OPV devices using P3HT/SPF Graphene as the active layer [5]. The detailed results were summarized in Table 4.2. The P3HT/SPF Graphene-based OPV devices also showed good OPV performance and similar graphene loading and annealing treatment dependence as for the P3OT/SPF Graphene-based

Table 4.2 Performance details (V_{oc} , J_{sc} , FF, and η) of the P3HT/graphene-based photovoltaic devices without annealing and after annealing at 160 and 210 °C for 10 and 20 min under a simulated AM 1.5G 100 mW illumination. Reproduced with permission [5]. Copyright 2009, Wiley-VCH

SPFGraphene content (%)	Annealing		V_{oc} (V)	J_{sc} (mA/cm ²)	FF	PCE %
	Temperature(°C)	Time(min)				
0	–	–	0.42	0.04	0.27	0.005
2.5	–	–	0.84	0.48	0.23	0.09
5	–	–	0.88	0.364	0.28	0.10
10	–	–	1.10	0.46	0.30	0.15
15	–	–	0.72	0.75	0.25	0.13
2.5	160	10	0.78	2.9	0.24	0.54
5	160	10	0.86	2.7	0.30	0.69
10	160	10	0.72	4.0	0.38	1.10
15	160	10	0.78	2.1	0.21	0.35
2.5	160	20	0.66	4.1	0.25	0.68
5	160	20	0.78	2.6	0.31	0.63
10	160	20	0.88	3.3	0.39	1.10
15	160	20	0.72	1.8	0.27	0.35
2.5	210	10	0.56	2.4	0.25	0.33
5	210	10	0.58	2.7	0.26	0.40
10	210	10	0.40	5.6	0.25	0.57
15	210	10	0.36	3.5	0.35	0.23
2.5	210	20	0.42	2.8	0.23	0.27
5	210	20	0.34	4.7	0.24	0.39
10	210	20	0.48	3.8	0.26	0.47
15	210	20	0.44	1.6	0.26	0.18

ones were observed. The highest PCE 1.10 % was obtained, which was slightly lower than that for the P3OT-based devices.

In addition, with a high specific surface area for a large interface, high mobility and tunable band gap, graphene quantum dots (GQDs) exhibit great potential as an electron acceptor in photovoltaic devices. Li et al. report an electrochemical approach for the direct preparation of functional GQDs with a uniform size of 3–5 nm, exhibiting a green luminescence and good stability [51]. Using these GQDs as the acceptor, devices with the structure of ITO/PEDOT:PSS/P3HT:GQDs/Al were fabricated. The best performance with a PCE of 1.28 %, J_{sc} of 6.33 mA/cm², V_{oc} of 0.67 V and FF 0.3 was achieved, which is comparable with most organic photovoltaic cells with electron acceptors other than fullerenes. Most recently, Gupta et al. employed aniline functionalized GQDs prepared from GSs by a hydrothermal approach as the acceptor to fabricate organic solar cells (Fig. 4.7) [52]. P3HT/ANI-GQD-based hybrid solar cells were fabricated with the device structure ITO/PEDOT:PSS/P3HT:ANI-GQDs/LiF/Al. Best performance with a PCE of 1.14 %, V_{oc} of 0.61 V, J_{sc} of 3.51 mA/cm², and FF of 0.53 were obtained for 1 wt% ANI-GQD in P3HT.

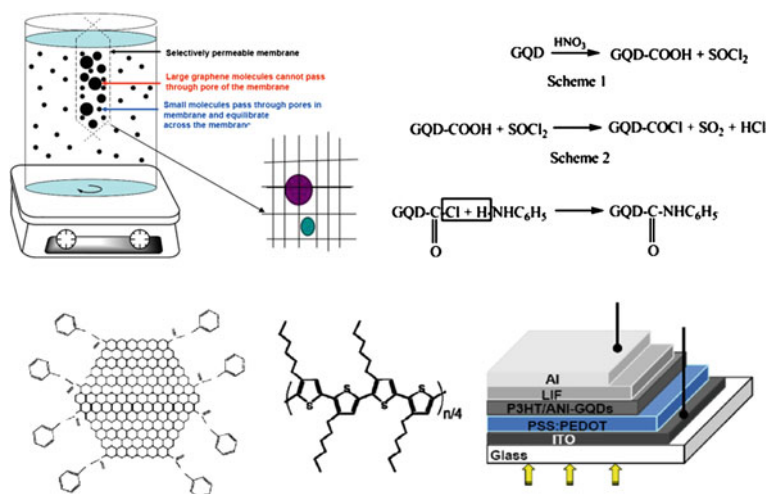


Fig. 4.7 **a** Schematic diagram of the graphene dialysis process. **b** Scheme of functionalization of graphene quantum dot (GQD) with aniline (ANI). **c**, **d** The idealized chemical structure of ANI-GQD and P3HT. **e** Schematic of the device with P3HT/ANI-GQD thin film as the active layer and the structure ITO/PEDOT:PSS (100 nm)/P3HT:ANI-GQD (100 nm)/LiF (1 nm)/Al (70 nm). Reproduced with permission [52]. Copyright 2011, ACS

The study using graphene as acceptor materials has just begun and the performance of OPVs employing graphene as the acceptor is still lower than that of fullerene derivatives. But, considering the intrinsic and superior properties of graphene, it is believed extremely important to advance the studies in this direction. In this regard, several factors are worth being considered: (1) the size of graphene. For the BHJ structure devices, the donor–acceptor (D–A) interface should be maximized for efficient exciton dissociation, and a nanoscale interpenetrating network should be formed for efficient charge transport to the electrodes. Thus, a proper size of graphene relative to the donor molecular size is important to form a well D–A interface and nanoscale interpenetrating network. (2) The functionalization of graphene and its batch-to-batch reproducibility. It is necessary to functionalize graphene in order to fabricate the device by solution process. In general, the performance of organic solar cell is very sensitive to even extremely little change of each materials and fabrication steps, especially for the active layer. Thus, the batch-to-batch reproducibility of both graphene and the functionalized graphene is important. (3) The HOMO/LUMO matching between graphene acceptor and the donors. The energy level of graphene and functionalized graphene are more-or-less different owing to their different sizes, layer structures, and reduction degrees. In addition, design and synthesis of new donor polymers matching graphene-based acceptor’s energy level are necessary because most of the donors nowadays are designed based on the acceptor of fullerene derivatives.

4.4 Graphene for All-Carbon Electronics

With its remarkable electronic and mechanical properties, graphene exhibits great potential in the preparation of all-carbon electronics. For the research of low-cost and flexible all-carbon devices or integrated circuits (ICs) based on graphene, one key is to develop an easy method to fabricate the device with simple process such as spin coating, inkjet printing, etc. Graphene films prepared by reduction of graphene oxide demonstrate some great advantages, especially when they are used as electrode materials with transparency requirement. In this section, we will give a brief introduction of graphene-based all-carbon electronics mainly based on our recent works.

4.4.1 All-Carbon Flexible FET

OFETs are the essential building blocks for state-of-the-art and next-generation electronics, which exhibit the advantages of low cost, large-area flexibility, etc. To fully exploit these advantages in practical applications, solution fabrication processes are strongly desired. Currently, metals like gold (Au) are widely used for the source/drain (S/D) electrodes in the fabrication of OFETs on SiO₂/Si substrates with doping Si as the gate (G) electrode, which make it difficult to achieve fully flexible, solution-processed, and low-cost devices. Thus, electrode materials with high carrier injection efficiency, excellent interface compatibility with organic semiconductors, and, especially, easy solution processability and suitability for use in flexible electronics are in high demand. As an alternative electrode material, graphene has demonstrated great potential to fulfill above requirements. Bao et al. have reported that OFET devices fabricated with rGO as bottom-contact electrodes have been demonstrated with lower contact resistances compared with those fabricated with gold contacts and desirable morphological features [53]. Recently, our group has fabricated OFETs using rGO for all the electrodes (source, drain, and gate) for the first time [54]. Patterned graphene electrodes and OFETs were fabricated as outlined in Fig. 4.8, Graphene was used for all S/D/G electrodes, and polyimide (PI) was used as the dielectric layer. In the device fabrication, the G electrode (graphene), dielectric layer PI, and S/D electrodes (graphene) were all fabricated by solution processes on a flexible PI substrate. These OFETs show performance comparable to corresponding devices using Au electrodes as the S/D electrodes on SiO₂/Si substrates with n-doped Si as the gate electrode. Also, these devices demonstrate excellent flexibility without performance degradation over severe bending cycles.

4.4.2 All-Carbon Flexible OPV

For all-carbon flexible OPV, metal electrodes should not be incorporated in the device. As discussed above, graphene acts as window electrode, the back electrode

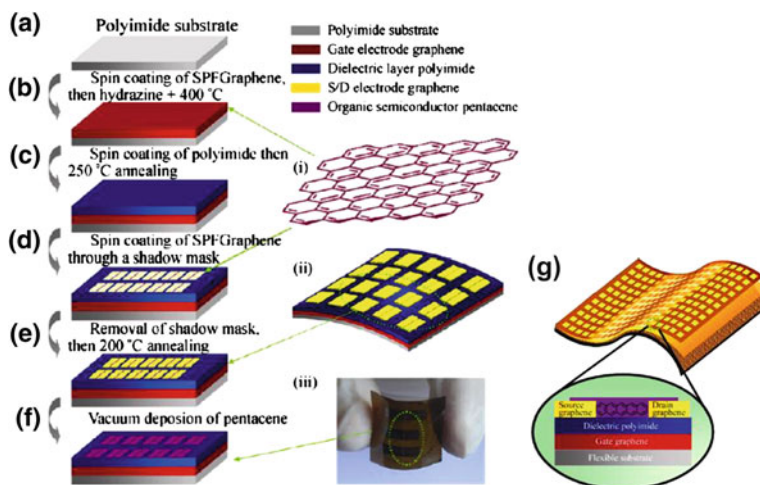


Fig. 4.8 (a–f) Schematic illustration of the fabrication of pentacene OFET devices. (i) Structure of graphene; (ii) a schematic representation of the unfinished OFET before adding the pentacene layer, showing its good flexibility; (iii) the finished pentacene OFET on a flexible PI substrate when bent under force. (g) A schematic illustration of the structure of flexible bottom-contact OFETs based on a pentacene film. Reproduced with permission [54]. Copyright 2011, Springer

is generally Al. Recently, Lee et al. reported a semitransparent inverted-type polymer solar cell using a top laminated graphene electrode [55]. The device was fabricated with a standard inverted structure using ZnO as electron transport layer, replacing the PEDOT:PSS hole-transporting layer by GO and the top metal electrode by the laminated CVD graphene film (Fig. 4.9a). The detailed fabrication process was presented in Fig. 4.9b. The resulting device structure was ITO/ZnO/P3HT:PCBM/GO/graphene. As illuminated from the ITO side, the semitransparent device achieves a best PCE of 2.50 % when the top electrode with 10 layers of graphene was employed, corresponding to 76 % of that of the standard opaque cell. The detailed performances were summarized in Table 4.3. Similar work has also been reported by Cox et al. using CVD graphene as back electrode for small molecule OPV device [56]. These results indicate that besides employed as window electrode in OPV, it can be used as back electrode. So, flexible, all-carbon solar cells can be constructed using graphene as both anode and cathode.

4.4.3 All-Carbon Conductive Circuit

From solution-processing graphene films, we fabricated various graphene-based microcosmic patterns and structures by computer controlled laser cutting (Fig. 4.10a–d, steps i–v) [57]. Furthermore, a complete working prototype of a flexible WORM memory card coupled with a real data retrieving system

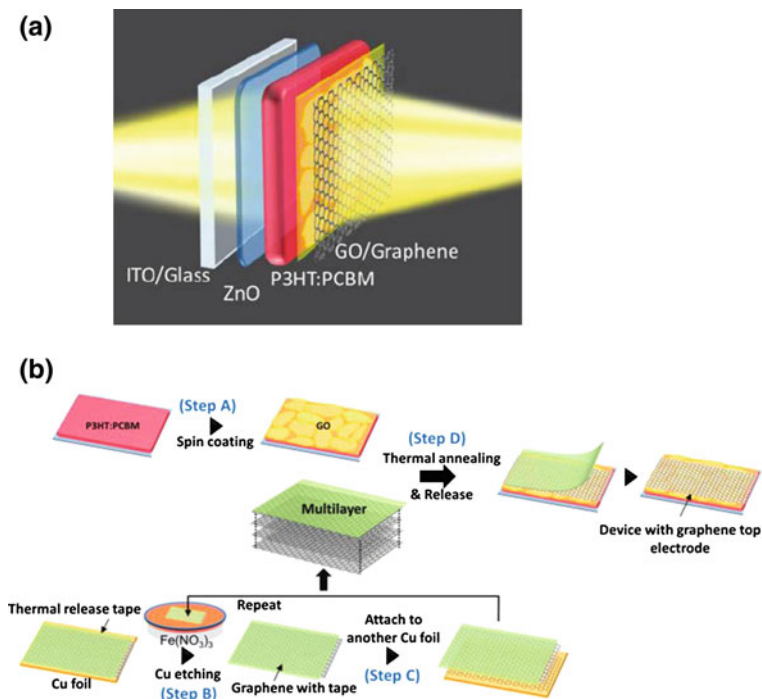


Fig. 4.9 **a** Semitransparent inverted polymer solar cell with a structure of ITO/ZnO/P3HT:PCBM/graphene oxide (GO)/graphene top electrode. **b** Fabrication of the ITO/ZnO/P3HT:PCBM/GO device before depositing the top electrode (step A). Top lamination processes of graphene electrodes by the graphene film transferring (steps B, C) and thermal annealing/releasing processes (step D). **a** Reproduced with permission [55]. Copyright 2011, ACS **b** Reproduced with permission [56]. Copyright 2011 AIP

Table 4.3 Summary of the device performances of the semitransparent polymer solar cells under illumination (AM1.5G, 100 mW/cm²) from the ITO side and the graphene side (parentheses) and the device performance of the reference standard opaque device

ITO (grapheme)	V_{oc} (V)	J_{sc} (mA/cm ²)	FF	PCE %
10 layers	0.54 (0.54)	10.50 (7.53)	0.44 (0.47)	2.50 (1.88)
8 layers	0.54 (0.54)	10.10 (7.70)	0.44 (0.49)	2.40 (2.04)
6 layers	0.54 (0.54)	8.62 (5.71)	0.39 (0.44)	1.82 (1.36)
3 layers	0.54 (0.54)	4.05 (3.19)	0.32 (0.33)	0.69(0.57)
Standard cell (Ag electrode)	0.52	11.5	0.55	3.30

constructed by maskless laser writing to store data directly has been demonstrated. The data density reaches 500,000 bits/cm² using our current very limited processing ability. The data storage has a high ON/OFF ratio and almost infinite lifetime.

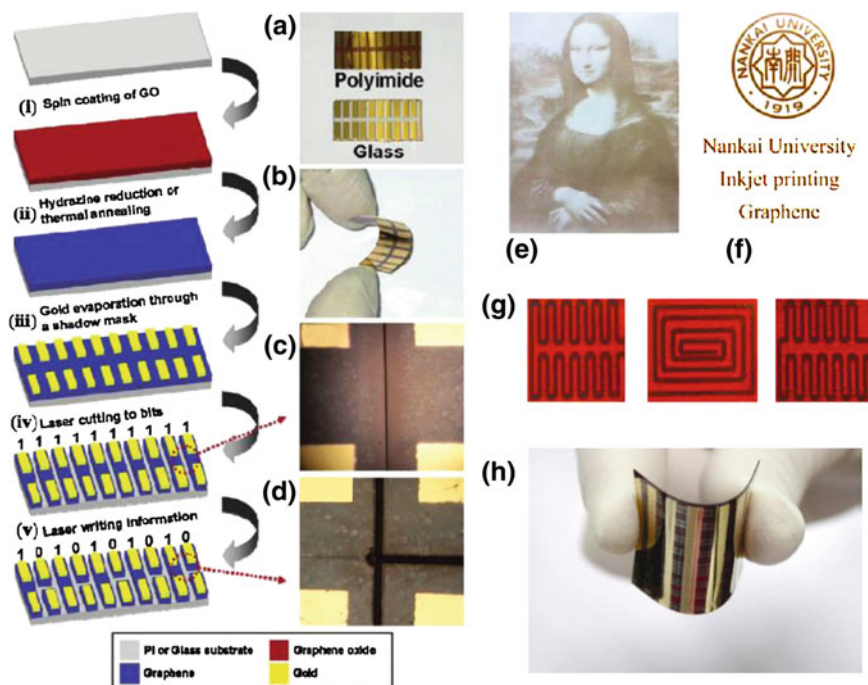


Fig. 4.10 Steps i–v: Schematic illustrations and photographs of the fabrication of a prototypical graphene-based WORM memory card with 10 bits. **a** Optical image for graphene films on flexible PI and glass substrates patterned with 10 pairs of gold electrodes. **b** Device on the PI substrate that exhibits well flexibility. **c** and **d** Optical microscope images of the laser-cutting channels for the prototypical graphene-based WORM memory card on a flexible PI substrate. The light part is the gold electrode, and the black lines are the cut channels. **e–g** Different patterns printed on various substrates by using GO or FGO inks with high resolution: patterns printed **e** on normal office printing paper using FGO ink with a concentration of 5 mg/mL. **f** on PET using GO ink with a concentration of 9 mg/mL. **g** on PI using FGO ink with a concentration of 5 mg/mL. **h** Photograph of a printed pattern on a PI substrate bent outwards by nearly 75°. The FGO ink printed pattern was reduced by thermal annealing. (i–v and a–d) Reproduced with permission [57]. Copyright 2011, ACS. e–h) Reproduced with permission [58]. Copyright 2011, Springer

Printing techniques, such as inkjet printing, are competitive alternatives to conventional photolithography for the production of electronic devices with advantages including low cost, ease of mass production, and flexibility. In contrast with conventional ink materials, such as metals like Au and Ag, CNTs and conducting materials, graphene-based inks demonstrate great advantages such as low cost, water solution process and high dispersity, etc. We reported a series of inkjet printing processes using graphene-based inks [58]. Under optimized conditions, using water-soluble single-layered GO and few-layered GO, various high image quality patterns could be printed on diverse flexible substrates, including paper, PET and PI, with the simple inkjet printing technique (Fig. 4.10e–h).

The graphene-based patterns printed on plastic substrates demonstrated a high electrical conductivity after thermal reduction, and more importantly, they retained the same conductivity over severe bending cycles (Fig. 4.10h). Accordingly, flexible electric circuits and a hydrogen peroxide chemical sensor were fabricated and showed excellent performances, demonstrating the applications of this simple and practical inkjet printing technique using graphene inks.

These results indicate that graphene could be an ideal material for fabricating the highly demanded all-carbon, flexible devices and electronics using the simple and efficient printing and spin-coating process and that the long-sought dream for all-carbon and flexible electronics is now much closer to reality.

4.5 Conclusion

In this chapter, transparent electrodes based on graphene and application of graphene in the electronic devices, especially OPVs, have been discussed. For transparent electrode, graphene has exhibited great potentials and achieved promising initial results. Improving the conductivity without sacrifice of the transparency is the first consideration for the further study. For OPVs using graphene as the transparent electrode or acceptor materials, the performance is still lower than that using the conventional materials. However, the performance such as PCE is more a device parameter than an intrinsic material parameter. Keep in mind that all the studies have been in the very initial stage for only 2–3 years. Therefore, there is great room for the improvement of the devices performance including that of all-carbon electronic devices. We fully expect that graphene is a great promising material in organic electronic devices and more and more exciting research results would be achieved in this direction.

Acknowledgments The authors gratefully acknowledge financial support from the NSFC (Grants 50933003, 50902073 and 50903044), MOST (Grants 2009AA032304, 2011CB932602 and 2011DFB50300) and NSF of Tianjin City (Grant 10ZCGHHZ00600)

References

1. Geim AK, Novoselov KS (2007) The rise of graphene. *Nat Mater* 6:183–191
2. Bonaccorso F, Sun Z, Hasan T, Ferrari AC (2010) Graphene photonics and optoelectronics. *Nat Photonics* 4:611–622
3. Liu Q, Liu ZF, Zhang XY, Zhang N, Yang LY, Yin SG, Chen Y (2008) Organic photovoltaic cells based on an acceptor of soluble graphene. *Appl Phys Lett* 92:223303
4. Liu ZF, Liu Q, Huang Y, Ma YF, Yin SG, Zhang XY, Sun W, Chen YS (2008) Organic photovoltaic devices based on a novel acceptor material: graphene. *Adv Mater* 20:3924–3930
5. Liu Q, Liu ZF, Zhong XY, Yang LY, Zhang N, Pan GL, Yin SG, Chen Y, Wei J (2009) Polymer photovoltaic cells based on solution-processable graphene and P3HT. *Adv Funct Mater* 19:894–904

6. Wu JB, Agrawal M, Becerril HA, Bao Z, Liu ZF, Chen Y, Peumans P (2010) Organic light-emitting diodes on solution-processed graphene transparent electrodes. *ACS Nano* 4:43–48
7. Matyba P, Yamaguchi H, Eda G, Chhowalla M, Edman L, Robinson ND (2010) Graphene and mobile ions: the key to all-plastic, solution-processed light-emitting devices. *ACS Nano* 4:637–642
8. Di CA, Wei DC, Yu G, Liu YQ, Guo YL, Zhu DB (2008) Patterned graphene as source/drain electrodes for bottom-contact organic field-effect transistors. *Adv Mater* 20:3289–3293
9. Pang SP, Tsao HN, Feng XL, Müllen K (2009) Patterned graphene electrodes from solution-processed graphite oxide films for organic field-effect transistors. *Adv Mater* 21:3488–3491
10. Rao CNR, Sood AK, Subrahmanyam KS, Govindaraj A (2009) Graphene: the new two-dimensional nanomaterial. *Angew Chem Int Ed* 48:7752–7777
11. Allen MJ, Tung VC, Kaner RB (2010) Honeycomb carbon: a review of graphene. *Chem Rev* 110:132–145
12. Huang X, Yin ZY, Wu SX, Qi XY, He QY, Zhang QC, Yan QY, Boey F, Zhang H (2011) Graphene-based materials: synthesis, characterization, properties and applications. *Small* 7:1876–1902
13. Hu YH, Wang H, Hu B (2010) Thinnest two-dimensional nanomaterial-graphene for solar energy. *ChemSusChem* 3:782–796
14. Liang MH, Luo B, Zhi LJ (2009) Application of graphene and graphene-based materials in clean energy-related devices. *Int J Energy Res* 33:1161–1170
15. Sun YQ, Wu QO, Shi GQ (2011) Graphene based new energy materials. *Energy Environ Sci* 4:1113–1132
16. Wassei JK, Kaner RB (2010) Graphene, a promising transparent conductor. *Mater Today* 13:52–59
17. Pang S, Hernandez Y, Feng X, Müllen K (2011) Graphene as transparent electrode material for organic electronics. *Adv Mater* 23:2779–2795
18. Novoselov KS, Geim AK, Morozov SV, Jiang D, Zhang Y, Dubonos SV, Grigorieva IV, Firsov AA (2004) Electric field effect in atomically thin carbon films. *Science* 306:666–669
19. Forbeaux I, Themlin JM, Debever JM (1998) Heteroepitaxial graphite on 6H-SiC(0001): interface formation through conduction-band electronic structure. *Phys Rev B* 58:16396–16406
20. Kim KS, Zhao Y, Jang H, Lee SY, Kim JM, Kim KS, Ahn JH, Kim P, Choi JY, Hong BH (2009) Large-scale pattern growth of graphene films for stretchable transparent electrodes. *Nature* 457:706–710
21. Dikin DA, Stankovich S, Zimney EJ, Piner RD, Dommett GH, Evmenenko G, Nguyen ST, Ruoff RS (2007) Preparation and characterization of graphene oxide paper. *Nature* 448:457–460
22. Eda G, Chhowalla M (2010) Chemically derived graphene oxide: towards large-area thin-film electronics and optoelectronics. *Adv Mater* 22:2392–2415
23. Park S, Ruoff RS (2009) Chemical methods for the production of graphenes. *Nat Nanotech* 4:217–224
24. Becerril HA, Mao J, Liu Z, Stoltenberg RM, Bao Z, Chen Y (2008) Evaluation of solution-processed reduced graphene oxide films as transparent conductors. *ACS Nano* 2:463–470
25. Xu Y, Long G, Huang L, Huang Y, Wan X, Ma Y, Chen Y (2010) Polymer photovoltaic devices with transparent graphene electrodes produced by spin-casting. *Carbon* 48:3308–3311
26. Wu J, Becerril HA, Bao Z, Liu Z, Chen Y, Peumans P (2008) Organic solar cells with solution-processed graphene transparent electrodes. *Appl Phys Lett* 92:263302
27. Eda G, Lin YY, Miller S, Chen CW, Su WF, Chhowalla M (2008) Transparent and conducting electrodes for organic electronics from reduced graphene oxide. *Appl Phys Lett* 92:23305
28. Yin ZY, Sun SY, Salim T, Wu SX, Huang XA, He QY, Lam YM, Zhang H (2010) Organic photovoltaic devices using highly flexible reduced graphene oxide films as transparent electrodes. *ACS Nano* 4:5263–5268
29. Geng JX, Liu LJ, Yang SB, Youn SC, Kim DW, Lee JS, Choi JK, Jung HT (2010) A simple approach for preparing transparent conductive graphene films using the controlled chemical

- reduction of exfoliated graphene oxide in an aqueous suspension. *J Phys Chem C* 114:14433–14440
30. De Arco LG, Zhang Y, Kumar A, Zhou CW (2009) Synthesis, transfer, and devices of single- and few-layer graphene by chemical vapor deposition. *IEEE T Nanotechnol* 8:135–138
 31. Yu QK, Lian J, Siriponglert S, Li H, Chen YP, Pei SS (2008) Graphene segregated on Ni surfaces and transferred to insulators. *Appl Phys Lett* 93:113103
 32. Reina A, Jia XT, Ho J, Nezich D, Son HB, Bulovic V, Dresselhaus MS, Kong J (2009) Large area, few-layer graphene films on arbitrary substrates by chemical vapor deposition. *Nano Lett* 9:30–35
 33. Wang Y, Chen XH, Zhong YL, Zhu FR, Loh KP (2009) Large area, continuous, few-layered graphene as anodes in organic photovoltaic devices. *Appl Phys Lett* 95:063302
 34. De Arco LG, Zhang Y, Schlenker CW, Ryu K, Thompson ME, Zhou CW (2010) Continuous, highly flexible, and transparent graphene films by chemical vapor deposition for organic photovoltaics. *ACS Nano* 4:2865–2873
 35. Wang Y, Tong SW, Xu XF, Özyilmaz B, Loh KP (2011) Interface engineering of layer-by-layer stacked graphene anodes for high-performance organic solar cells. *Adv Mater* 23:1514–1518
 36. Choe M, Lee BH, Jo G, Park J, Park W, Lee S, Hong WK, Seong MJ, Kahng YH, Lee K, Lee T (2010) Efficient bulk-heterojunction photovoltaic cells with transparent multi-layer graphene electrodes. *Org Electron* 11:1864–1869
 37. Xu Y, Wang Y, Liang J, Huang Y, Ma Y, Wan X, Chen Y (2009) Hybrid material of graphene and poly(3,4-ethyldioxythiophene) with high conductivity, flexibility, and transparency. *Nano Res* 2:343–348
 38. Dai B, Fu L, Liao L, Liu N, Yan K, Chen Y, Liu Z (2011) High-quality single-layer graphene via reductive reduction of graphene oxide. *Nano Res* 4:434–439
 39. Tung VC, Chen LM, Allen MJ, Wassei JK, Nelson K, Kaner RB, Yang Y (2009) Low-temperature solution processing of graphene-carbon nanotube hybrid materials for high-performance transparent conductors. *Nano Lett* 9:1949–1955
 40. Wildoer JWG, Venema LC, Rinzler AG, Smalley RE, Dekker C (1998) Electronic structure of atomically resolved carbon nanotubes. *Nature* 391:59–62
 41. Huang JH, Fang JH, Liu CC, Chu CW (2011) Effective work function modulation of graphene/carbon nanotube composite films as transparent cathodes for organic optoelectronics. *ACS Nano* 5:6262–6271
 42. Jo G, Na SI, Oh SH, Lee S, Kim TS, Wang G, Choe M, Park W, Yoon J, Kim DY, Kahng YH, Lee T (2010) Tuning of a graphene-electrode work function to enhance the efficiency of organic bulk heterojunction photovoltaic cells with an inverted structure. *Appl Phys Lett* 97:213301
 43. Cheng YJ, Yang SH, Hsu CS (2009) Synthesis of conjugated polymers for organic solar cell applications. *Chem Rev* 109:5868–5923
 44. Chen JW, Cao Y (2009) Development of novel conjugated donor polymers for high-efficiency bulk-heterojunction photovoltaic devices. *Acc Chem Res* 42:1709–1718
 45. Anthony JE (2011) Small-molecule, nonfullerene acceptors for polymer bulk heterojunction organic photovoltaics. *Chem Mater* 23:583–590
 46. Liu YX, Summers MA, Scully SR, McGehee MD (2006) Resonance energy transfer from organic chromophores to fullerene molecules. *J Appl Phys* 99:093521
 47. He YJ, Li YF (2011) Fullerene derivative acceptors for high performance polymer solar cells. *Phys Chem Chem Phys* 13:1970–1983
 48. Brunetti FG, Gong X, Tong M, Heeger AJ, Wudl F (2010) Strain and huckel aromaticity: driving forces for a promising new generation of electron acceptors in organic electronics. *Angew Chem Int Ed* 49:532–536
 49. Brunetti FG, Kumar R, Wudl F (2010) Organic electronics from perylene to organic photovoltaics: painting a brief history with a broad brush. *J Mater Chem* 20:2934–2948
 50. Hill CM, Zhu Y, Pan S (2011) Fluorescence and electroluminescence quenching evidence of interfacial charge transfer in poly(3-hexylthiophene): graphene oxide bulk heterojunction photovoltaic devices. *ACS Nano* 5:942–951

51. Li Y, Hu Y, Zhao Y, Shi GQ, Deng LE, Hou YB, Qu LT (2011) An electrochemical avenue to green-luminescent graphene quantum dots as potential electron-acceptors for photovoltaics. *Adv Mater* 23:776–780
52. Gupta V, Chaudhary N, Srivastava R, Sharma GD, Bhardwaj R, Chand S (2011) Luminescent graphene quantum dots for organic photovoltaic devices. *J Am Chem Soc* 133:9960–9963
53. Becerril HA, Stoltenberg RM, Tang ML, Roberts ME, Liu ZF, Chen Y, Kim DH, Li BL, Lee SY, Bao Z (2010) Fabrication and evaluation of solution-processed reduced graphene oxide electrodes for p- and n-channel bottom-contact organic thin-film transistors. *ACS Nano* 4:6343–6352
54. Chen Y, Xu Y, Zhao K, Wan X, Deng J, Yan W (2010) Towards flexible all-carbon electronics: flexible organic field-effect transistors and inverter circuits using solution-processed all-graphene source/drain/gate electrodes. *Nano Res* 3:675–684
55. Lee YY, Tu KH, Yu CC, Li SS, Hwang JY, Lin CC, Chen KH, Chen LC, Chen CW (2011) Top laminated graphene electrode in a semitransparent polymer solar cell by simultaneous thermal annealing/releasing method. *ACS Nano* 5:6564–6570
56. Cox M, Gorodetsky A, Kim B, Kim KS, Jia Z, Kim P, Nuckolls C, Kymissis I (2011) Single-layer graphene cathodes for organic photovoltaics. *Appl Phys Lett* 98:123303
57. Liang J, Chen Y, Xu Y, Liu Z, Zhang L, Zhao X, Zhang X, Tian J, Huang Y, Ma Y, Li F (2011) Toward all-carbon electronics: fabrication of graphene-based flexible electronic circuits and memory cards using maskless laser direct writing. *ACS Appl Mater Interfaces* 2:3310–3317
58. Huang L, Huang Y, Liang J, Wan X, Chen Y (2011) Graphene-based conducting inks for direct inkjet printing of flexible conductive patterns and their applications in electric circuits and chemical sensors. *Nano Res* 4:675–684